stimulation intensity is feedback-controlled continuously, the therapeutic effect and safety could be enhanced.

Quantification of the dynamic characteristics of a target system is the first step for developing a robust controller [42–44]. Next, the controller should be designed in such a way that the variation of the target system dynamics does not affect the controlling result much [45]. The simulation of the closed-loop AP response in CHF, such as that shown in Fig. 5, will be utilized in designing a robust controller system of the carotid sinus activation.

Limitations

First, we used normal rats without sham operation as the control group. Sham-operated rats may serve as a more appropriate control. Although the surgical operation of thoracotomy itself could have affected the baroreflex function in the CHF group, because over 100 days had elapsed after the surgical operation, the effect of surgical operation might have been limited. Actually, two rats that underwent coronary ligation but did not meet the criteria for CHF retained the maximum gain of the total baroreflex close to the control group (rat A: central venous pressure = 2.28 mmHg, biventricular weight = 1.94 g kg^{-1}, total baroreflex gain = 1.61; rat B: central venous pressure = 1.69 mmHg, biventricular weight = 2.33 g kg^{-1}, total baroreflex gain = 1.67).

Second, the data were obtained under anesthetic conditions. Because the anesthesia affects autonomic nervous activities, the results should be carefully interpreted. Vagotomy and lower perfusion of the brain due to carotid artery occlusion might have also affected the baroreflex function. Nevertheless, the present results would provide a unique clue to integrated understanding of the impaired baroreflex function in CHF.

Third, we did not measure cardiac output or peripheral vascular resistance. Subdividing the peripheral arc into the cardiac and vascular components will be necessary to identify the mechanisms for an approximately linear relationship between SNA and AP in both the control and CHF rats.

Conclusions

The dynamic and static characteristics of the neural arc, peripheral arc, and total baroreflex were analyzed comprehensively in rats with CHF after myocardial infarction. Although the derivative characteristics of the baroreflex neural arc are preserved in the CHF rats, the dynamic AP regulation is depressed in both the magnitude and response speed. The equilibrium diagram indicates that the baroreflex gain may seem preserved in CHF in a small range around the closed-loop operating point. However, the percent recovery of AP and the speed of recovery are reduced progressively as the size of exogenous disturbance increases in the CHF rats. The reserve for AP buffering may be lost in CHF despite the relatively maintained baseline AP.

Acknowledgments This study was supported by Health and Labour Sciences Research Grants (H18-nano-Ippan-003, H19-nano-Ippan-009, H20-katsudo-Shitei-007, and H21-nano-Ippan-005) from the Ministry of Health, Labour and Welfare of Japan; by a Grant-in-Aid for Scientific Research (No. 20390462) from the Ministry of Education, Culture, Sports, Science and Technology of Japan; and by the Industrial Technology Research Grant Program from the New Energy and Industrial Technology Development Organization (NEDO) of Japan.

Appendix 1: feature of a Gaussian white noise input

The neural arc of the arterial baroreflex may be roughly modeled by a cascade system, which consists of a dynamic linear subsystem followed by a static nonlinear subsystem [14]. In this type of system, the selection of the mean input pressure and the amplitude of input does not significantly affect the estimation of the system linear dynamics except for a factor of proportionality when the system is tested with a Gaussian white noise (GWN) signal [46]. In order to demonstrate the above notion, we performed a simulation study. In reference to Fig. 6a, the dynamic linear subsystem for the baroreflex neural arc was modeled by the following equation:

$$H_N(f) = \frac{1+\frac{f}{f_{C1}}j}{\left(1+\frac{f}{f_{C2}}j\right)^2}\exp(-2\pi fjL) \tag{5}$$

where f_{C1} and f_{C2} are the corner frequencies determining the frequency-dependent changes in the dynamic gain, L denotes the pure dead time, f and j indicate frequency and an imaginary unit, respectively. We set $f_{C1} = 0.1$ Hz, $f_{C2} = 0.9$ Hz, and $L = 0.1$ s to mimic the neural arc transfer function. The static nonlinear subsystem of the neural arc was modeled by the logistic function (Eq. 3) with parameters of $P_1 = 60\%$, $P_2 = 0.1$ $mmHg^{-1}$, $P_3 = 120$ mmHg, and $P_4 = 40\%$. Using this model, the linear input-output relationship was estimated by a GWN input or a binary white noise (BIN) input. Mean input pressure was changed among 120, 90, and 150 mmHg (P_3, $P_3 - 30$, and $P_3 + 30$ mmHg).

Figure 6b through 6d shows the estimation results. In each panel, thin smooth curves in the gain and phase plots indicate the transfer function of the dynamic linear subsystem described by Eq. 5. The solid bold curves, dotted thin curves, and dashed thin curves represent the estimation

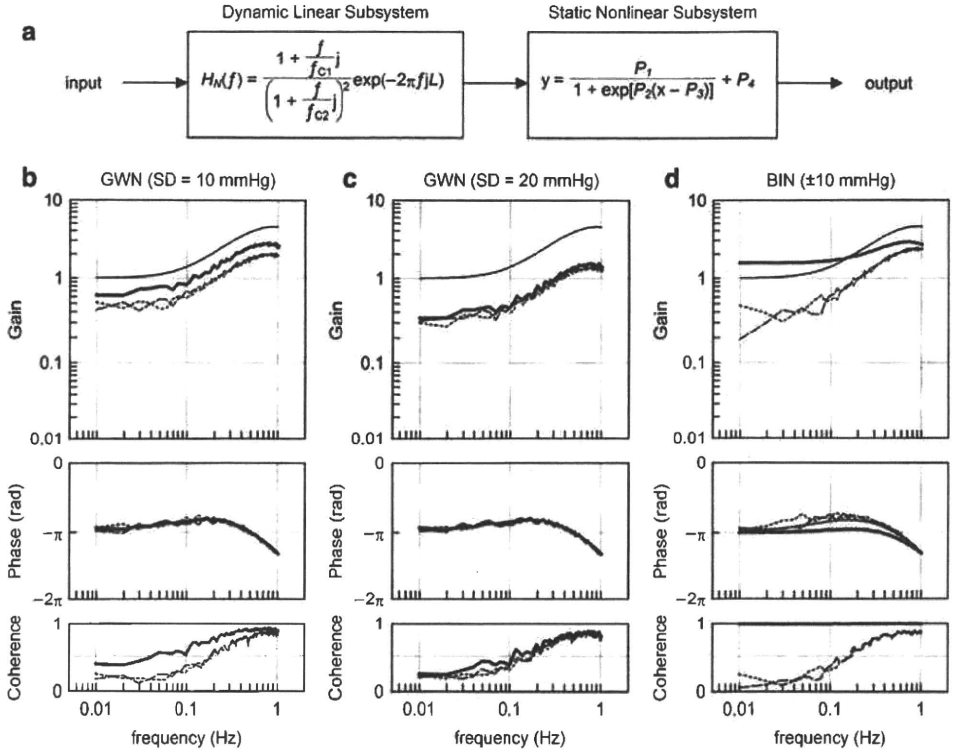

Fig. 6 **a** A cascade model for the baroreflex neural arc, which consists of a dynamic linear subsystem and a static nonlinear subsystem. The dynamic linear subsystem represents the neural arc transfer function. The static nonlinear subsystem represents the sigmoidal nonlinearity for the neural arc. **b** Estimation results of the system dynamic characteristics using a Gaussian white noise (GWN) input with a standard deviation (SD) of 10 mmHg. **c** Estimation results of the system dynamic characteristics using a GWN input with an SD of 20 mmHg. **d** Estimation results of the system dynamic characteristics using a binary white noise (BIN) input with an amplitude of 10 mmHg. In panels **b** through **d**, the *thin smooth curve* indicates the transfer function of the given dynamic linear subsystem. The *solid bold curve*, *dotted thin curve*, and *dashed thin curve* represent the estimation results obtained by the input signals with mean input pressures of 120, 90, and 150 mmHg, respectively (see text for explanation)

results obtained by mean input pressures of 120, 90, and 150 mmHg, respectively. Figure 6b and c represents the estimation results obtained by GWNs with standard deviations of 10 and 20 mmHg, respectively. As can be seen, the estimated gain plots are nearly parallel to the gain plot of the given dynamic linear subsystem. The estimated phase plots are superimposable on the phase plot of the given dynamic linear subsystem.

Figure 6d shows the estimation results obtained by BINs with an amplitude of 10 mmHg (i.e., the peak-to-peak pressure of 20 mmHg). None of the estimated gain plots are parallel to the gain plot of the given dynamic linear subsystem. The estimated phase plots also deviated from the phase plot of the given dynamic linear subsystem. When the system was tested by the BIN input with the mean input pressure of 120 mmHg, the coherence value became close to unity, suggesting that the BIN input had caused on-off behavior in the system output.

The above simulation results confirm that the selection of the mean input pressure and the amplitude of GWN does not significantly affect the estimation of the dynamic characteristics of the system except for a factor of proportionality when the mean input pressure and the standard deviation of GWN are not far beyond the system operating range.

Appendix 2: estimation of the initial slope of the step response or recovery response

To characterize the speed of the response, the initial slope of the response was calculated as follows. First, a response threshold is determined as the 5% value of the steady-state step response. In the case of the recovery response, 5% of the maximum recovery is used as the threshold. Next, an initial time point at which the response exceeds the threshold value is determined. Starting from this initial time point, a linear regression analysis giving a slope and an intercept is performed repeatedly while increasing the number of analyzed data points. The steepest slope thus

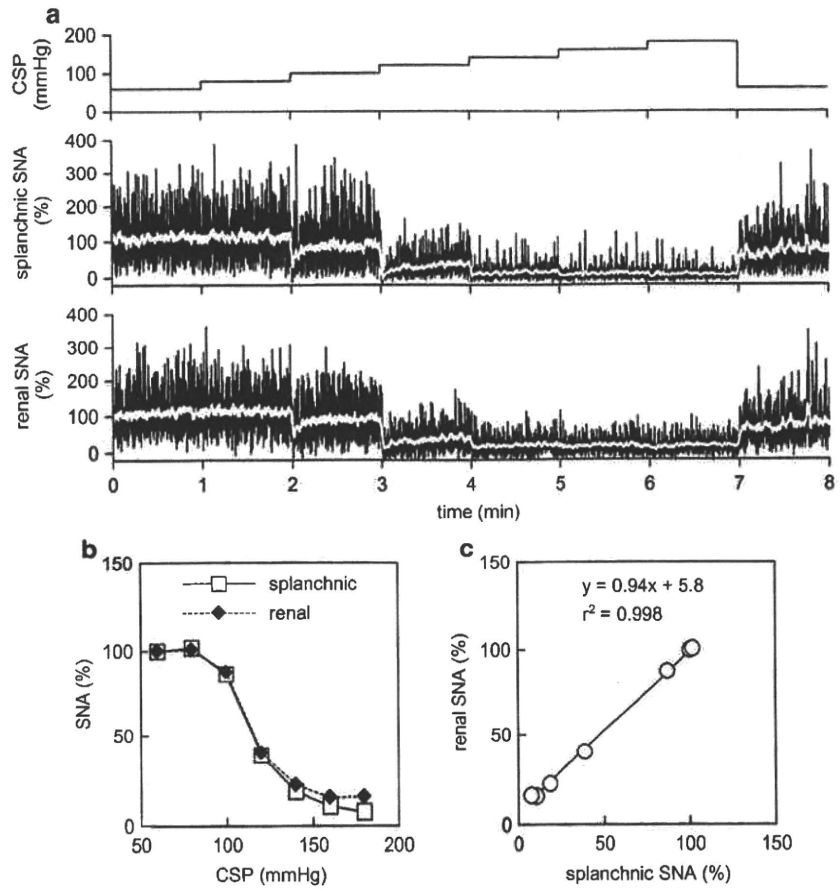

Fig. 7 **a** Typical recordings of 10-Hz decimated CSP, splanchnic SNA, and renal SNA obtained from a normal rat in an additional study using the same experimental settings as the main study. The *white lines* in the SNA recordings represent 2-s moving averaged signals. An increase in CSP decreased splanchnic and renal SNAs. **b** Static characteristics of the baroreflex neural arc drawn based on splanchnic and renal SNAs. **c** Correlation between splanchnic and renal SNAs during the stepwise input protocol. In panels **b** and **c**, splanchnic and renal SNA data were obtained as the averaged values during the last 10 s at each CSP level

obtained is used as the initial slope of the response. By setting the 5% threshold, the linear regression can be performed excluding the initial data points constituting the dead time.

Appendix 3: comparison of splanchnic and renal SNAs under the present experimental conditions

We compared splanchnic and renal SNAs under the present experimental conditions in an additional three rats. A branch of the right renal sympathetic nerve was exposed through a right flank incision, and renal SNA was recorded simultaneously with splanchnic SNA. Figure 7a presents time series of 10-Hz decimated CSP, splanchnic SNA, and renal SNA obtained from one rat. White lines in splanchnic and renal SNAs indicate 2-s moving averaged signals. In each of the splanchnic and renal SNAs, a 10-s averaged value for the last 10 s at CSP of 60 mmHg was defined as 100%, and a 10-s averaged value after the administration of hexamethonium bromide was defined as 0%, in the same manner as the main study. Figure 7b shows the relationships of SNAs versus CSP. Although the renal SNA values were slightly greater than the splanchnic SNA values at CSPs of 160 and 180 mmHg in this rat, the general sigmoidal relationships were similar between the two SNAs. The regression line for renal SNA (y) versus splanchnic SNA (x) was $y = 0.94x + 5.8$ ($r^2 = 0.998$) in this rat (Fig. 7c). The other two rats showed regression lines of $y = 1.01x + 0.3$ ($r^2 = 0.999$) and $y = 0.99x + 3.7$ ($r^2 = 0.995$), suggesting that both splanchnic and renal SNAs can represent common activity for the AP regulation during the stepwise input protocol under the present experimental conditions.

References

1. Ikeda Y, Kawada T, Sugimachi M, Kawaguchi O, Shishido T, Sato T, Miyano H, Matsuura W, Alexander J Jr, Sunagawa K (1996) Neural arc of baroreflex optimizes dynamic pressure regulation in achieving both stability and quickness. Am J Physiol 271:H882–H890
2. Sato T, Kawada T, Inagaki M, Shishido T, Sugimachi M, Sunagawa K (2003) Dynamics of sympathetic baroreflex control of arterial pressure in rats. Am J Physiol Regul Integr Comp Physiol 285:R262–R270
3. White CW (1981) Abnormalities in baroreflex control of heart rate in canine heart failure. Am J Physiol 240:H793–H799
4. Wang W, Chen JS, Zucker IH (1990) Carotid sinus baroreceptor sensitivity in experimental heart failure. Circulation 81:1959–1966

5. Wang W, Chen JS, Zucker IH (1991) Carotid sinus baroreceptor reflex in dogs with experimental heart failure. Circ Res 68:1294–1301
6. Wang W, Brändle M, Zucker IH (1993) Influence of vagotomy on the baroreflex sensitivity in anesthetized dogs with experimental heart failure. Am J Physiol 265:H1310–H1317
7. Li M, Zheng C, Sato T, Kawada T, Sugimachi M, Sunagawa K (2004) Vagal nerve stimulation markedly improves long-term survival after chronic heart failure in rats. Circulation 109:120–124
8. Shoukas AA, Callahan CA, Lash JM, Haase EB (1991) New technique to completely isolate carotid sinus baroreceptor regions in rats. Am J Physiol 260:H300–H303
9. Sato T, Kawada T, Miyano H, Shishido T, Inagaki M, Yoshimura R, Tatewaki T, Sugimachi M, Alexander J Jr, Sunagawa K (1999) New simple methods for isolating baroreceptor regions of carotid sinus and aortic depressor nerves in rats. Am J Physiol 276:H326–H332
10. Kawada T, Kamiya A, Li M, Shimizu S, Uemura K, Yamamoto H, Sugimachi M (2009) High levels of circulating angiotensin II shift the open-loop baroreflex control of splanchnic sympathetic nerve activity, heart rate and arterial pressure in anesthetized rats. J Physiol Sci 59:447–455
11. Marmarelis PZ, Marmarelis VZ (1978) The white noise method in system identification. In: Analysis of physiological systems. Plenum, New York, pp 131–221
12. Kent BB, Drane JW, Blumenstein B, Manning JW (1972) A mathematical model to assess changes in the baroreceptor reflex. Cardiology 57:295–310
13. Glantz SA (2002) Primer of biostatistics, 5th edn. McGraw-Hill, New York
14. Kawada T, Yanagiya Y, Uemura K, Miyamoto T, Zheng C, Li M, Sugimachi M, Sunagawa K (2003) Input-size dependence of the baroreflex neural arc transfer characteristics. Am J Physiol Heart Circ Physiol 284:H404–H415
15. Yamamoto K, Kawada T, Kamiya A, Takaki H, Shishido T, Sunagawa K, Sugimachi M (2008) Muscle mechanoreflex augments arterial baroreflex-mediated dynamic sympathetic response to carotid sinus pressure. Am J Physiol Heart Circ Physiol 295:H1081–H1089
16. Kamiya A, Kawada T, Yamamoto K, Mizuno M, Shimizu S, Sugimachi M (2008) Upright tilt resets dynamic transfer function of baroreflex neural arc to minify the pressure disturbance in total baroreflex control. J Physiol Sci 58:189–198
17. Mohrman DE, Heller LJ (2006) Cardiovascular physiology, 6th edn. McGraw Hill, New York
18. Sato T, Kawada T, Inagaki M, Shishido T, Takaki H, Sugimachi M, Sunagawa K (1999) New analytic framework for understanding sympathetic baroreflex control of arterial pressure. Am J Physiol 276:H2251–H2261
19. Lepage S (2008) Acute decompensated heart failure. Can J Cardiol 24(Suppl B):6B–8B
20. Masaki H, Imaizumi T, Harasawa Y, Takeshita A (1994) Dynamic arterial baroreflex in rabbits with heart failure induced by rapid pacing. Am J Physiol 267:H92–H99
21. Kawai H, Mohan A, Hagen J, Dong E, Armstrong J, Stevens SY, Liang CS (2000) Alterations in cardiac adrenergic terminal function and β-adrenoceptor density in pacing-induced heart failure. Am J Physiol Heart Circ Physiol 278:H1708–H1716
22. Kawada T, Shishido T, Inagaki M, Zheng C, Yanagiya Y, Uemura K, Sugimachi M, Sunagawa K (2002) Estimation of baroreflex gain using a baroreflex equilibrium diagram. Jpn J Physiol 52:21–29
23. Kashihara K, Kawada T, Li M, Sugimachi M, Sunagawa K (2004) Bezold-Jarisch reflex blunts arterial baroreflex via the shift of neural arc toward lower sympathetic nerve activity. Jpn J Physiol 54:395–404
24. Yamamoto K, Kawada T, Kamiya A, Takaki H, Miyamoto T, Sugimachi M, Sunagawa K (2004) Muscle mechanoreflex induces the pressor response by resetting the arterial baroreflex neural arc. Am J Physiol Heart Circ Physiol 286:H1382–H1388
25. Kamiya A, Kawada T, Yamamoto K, Michikami D, Ariumi H, Uemura K, Zheng C, Shimizu S, Aiba T, Miyamoto T, Sugimachi M, Sunagawa K (2005) Resetting of the arterial baroreflex increases orthostatic sympathetic activation and prevents postural hypotension in rabbits. J Physiol 566:237–246
26. Michikami D, Kamiya A, Kawada T, Inagaki M, Shishido T, Yamamoto K, Ariumi H, Iwase S, Sugenoya J, Sunagawa K, Sugimachi M (2006) Short-term electroacupuncture at Zusanli resets the arterial baroreflex neural arc toward lower sympathetic nerve activity. Am J Physiol Heart Circ Physiol 291:H318–H326
27. Ninomiya I, Nisimaru N, Irisawa H (1971) Sympathetic nerve activity to the spleen, kidney, and heart in response to baroceptor input. Am J Physiol 221:1346–1351
28. Matsukawa K, Ninomiya I, Nishiura N (1993) Effects of anesthesia on cardiac and renal sympathetic nerve activities and plasma catecholamines. Am J Physiol 265:R792–R797
29. Yamamoto H, Kawada T, Kamiya A, Kita T, Sugimachi M (2008) Electroacupuncture changes the relationship between cardiac and renal sympathetic nerve activities in anesthetized cats. Auton Neurosci 144:43–49
30. Rowell LB (1974) Human cardiovascular adjustments to exercise and thermal stress. Physiol Rev 54:75–159
31. Kawada T, Uemura K, Kashihara K, Jin Y, Li M, Zheng C, Sugimachi M, Sunagawa K (2003) Uniformity in dynamic baroreflex regulation of left and right cardiac sympathetic nerve activities. Am J Physiol Regul Integr Comp Physiol 284:R1506–R1512
32. Kawada T, Shishido T, Inagaki M, Tatewaki T, Zheng C, Yanagiya Y, Sugimachi M, Sunagawa K (2001) Differential dynamic baroreflex regulation of cardiac and renal sympathetic nerve activities. Am J Physiol Heart Circ Physiol 280:H1581–H1590
33. Kamiya A, Kawada T, Yamamoto K, Michikami D, Ariumi H, Miyamoto T, Shimizu S, Uemura K, Aiba T, Sunagawa K, Sugimachi M (2005) Dynamic and static baroreflex control of muscle sympathetic nerve activity (SNA) parallels that of renal and cardiac SNA during physiological change in pressure. Am J Physiol Heart Circ Physiol 289:H2641–H2648
34. Kassis E (1987) Cardiovascular response to orthostatic tilt in patients with severe congestive heart failure. Cardiovasc Res 21:362–368
35. Packer M, Fowler MB, Roecker EB, Coats AJ, Katus HA, Krum H, Mohacsi P, Rouleau JL, Tendera M, Staiger C, Holcslaw TL, Amann-Zalan I, DeMets DL (2002) Effect of carvedilol on the morbidity of patients with severe chronic heart failure: results of the Carvedilol Prospective Randomized Cumulative Survival (COPERNICUS) study. Circulation 106:2194–2199
36. Yusuf S, Sleight P, Pogue J, Bosch J, Davies R, Dagenais G (2000) Effects of an angiotensin-converting-enzyme inhibitor, ramipril, on cardiovascular events in high-risk patients. The heart outcomes prevention evaluation study investigators. N Engl J Med 342:145–153
37. Telmisartan Randomised AssessmeNt Study in ACE iNtolerant subjects with cardiovascular Disease (TRANSCEND) Investigators, Yusuf S, Teo K, Anderson C, Pogue J, Dyal L, Copland I, Schumacher H, Dagenais G, Sleight P (2008) Effects of the angiotensin-receptor blocker telmisartan on cardiovascular events in high-risk patients intolerant to angiotensin-converting enzyme inhibitors: a randomised controlled trial. Lancet 372:1174–1183

38. Schwartz PJ, De Ferrari GM, Sanzo A, Landolina M, Rordorf R, Raineri C, Campana C, Revera M, Ajmone-Marsan N, Tavazzi L, Odero A (2008) Long term vagal stimulation in patients with advanced heart failure: first experience in man. Eur J Heart Fail 10:884–891
39. Mancia G, Seravalle G, Giannattasio C, Bossi M, Preti L, Cattaneo BM, Grassi G (1992) Reflex cardiovascular control in congestive heart failure. Am J Cardiol 69:17G–23G
40. Eckberg DL, Drabinsky M, Braunwald E (1971) Defective cardiac parasympathetic control in patients with heart disease. N Engl J Med 285:877–883
41. Zucker IH, Hackley JF, Cornish KG, Hiser BA, Anderson NR, Kieval R, Irwin ED, Serdar DJ, Peuler JD, Rossing MA (2007) Chronic baroreceptor activation enhances survival in dogs with pacing-induced heart failure. Hypertension 50:904–910
42. Sato T, Kawada T, Sugimachi M, Sunagawa K (2002) Bionic technology revitalizes native baroreflex function in rats with baroreflex failure. Circulation 106:730–734
43. Gotoh TM, Tanaka K, Morita H (2005) Controlling arterial blood pressure using a computer-brain interface. Neuroreport 16:343–347
44. Kawada T, Shimizu S, Yamamoto H, Shishido T, Kamiya A, Miyamoto T, Sunagawa K, Sugimachi M (2009) Servo-controlled hind-limb electrical stimulation for short-term arterial pressure control. Circ J 73:851–859
45. Åström K, Hägglund T (1995) PID controllers: theory, design, and tuning, 2nd edn. International Society of Automation, Research Triangle Park, NC
46. Hunter IW, Korenberg MJ (1986) The identification of nonlinear biological systems: Wiener and Hammerstein cascade models. Biol Cybern 55:135–144

Autonomic Neuroscience: Basic and Clinical 156 (2010) 149–151

Contents lists available at ScienceDirect

Autonomic Neuroscience: Basic and Clinical

journal homepage: www.elsevier.com/locate/autneu

Short communication

Large conductance Ca^{2+}-activated K^+ channels inhibit vagal acetylcholine release at the rabbit sinoatrial node

Toru Kawada [a,*], Tsuyoshi Akiyama [b], Shuji Shimizu [a], Atsunori Kamiya [a], Kazunori Uemura [a], Yusuke Sata [a], Mikiyasu Shirai [b], Masaru Sugimachi [a]

[a] Department of Cardiovascular Dynamics, National Cerebral and Cardiovascular Center Research Institute, Osaka, Japan
[b] Department of Cardiac Physiology, National Cerebral and Cardiovascular Center Research Institute, Osaka, Japan

ARTICLE INFO

Article history:
Received 15 January 2010
Received in revised form 1 April 2010
Accepted 9 April 2010

Keywords:
Acetylcholine
Cardiac microdialysis
Vagal stimulation
Rabbits

ABSTRACT

Although large conductance Ca^{2+}-activated K^+ (BK) channels play an important role in determining vascular tone, their role in the efferent cardiac vagal system remains to be elucidated. In anesthetized rabbits ($n=9$), acetylcholine (ACh) was measured at the right atrium near the sinoatrial node by a cardiac microdialysis technique, and the ACh release in response to electrical stimulation of the cervical preganglionic vagal nerves was examined. Local administration of a BK channel blocker iberiotoxin (2 μM) through a dialysis fiber increased the stimulation-induced ACh release from 7.6 ± 2.7 to 9.0 ± 3.2 nM ($P<0.05$). Addition of intravenous administration of iberiotoxin (0.11 mg/body) did not increase the stimulation-induced ACh release further (10.8 ± 4.4 nM). These results indicate that the BK channels play an inhibitory role in the vagal ACh release to the sinoatrial node.

1. Introduction

Ca^{2+}-activated K^+ channels are located in the vicinity of voltage-dependent Ca^{2+} channels. Their activation induces outward efflux of K^+, leading to hyperpolarization of the plasma membrane and promoting closure of the voltage-dependent Ca^{2+} channels. Among the group of Ca^{2+}-activated K^+ channels, large conductance Ca^{2+}-activated K^+ channels, also designated as the "Big K" (BK) channels, are expressed in the plasma membrane of vascular smooth muscle cells and contribute to the regulation of vascular tone (Ledoux et al., 2006). The BK channels are also found on neural cells and play a critical role in shaping action potentials and modifying firing patterns (Pedarzani et al., 2000). Blockade of the BK channels by iberiotoxin enhanced presynaptic release of acetylcholine (ACh) and postsynaptic release of catecholamine in the rat adrenal medulla during electrical stimulation of the splanchnic nerve, suggesting an inhibitory role of the BK channels in the physiological catecholamine release from the adrenal medulla (Akiyama et al., 2010). The role of the BK channels in the efferent vagal system in controlling the heart, however, remains to be elucidated. If the BK channels limit Ca^{2+} entry through the voltage-dependent Ca^{2+} channels in the preganglionic and/or postganglionic vagal nerve terminals, blockade of the BK channels by iberiotoxin would enhance the ACh release in response to electrical stimulation of the preganglionic vagal nerve. A recent development of a cardiac microdialysis technique in the in vivo rabbit right atrium has enabled direct monitoring of vagal ACh release to the sinoatrial node (Shimizu et al., 2009). This technique was used to examine the role of the BK channels in the efferent cardiac vagal system.

2. Materials and methods

Animal care was conducted in accordance with the *Guiding Principles for the Care and Use of Animals in the Field of Physiological Sciences*, which has been approved by the Physiological Society of Japan. All experimental protocols were reviewed and approved by the Animal Subjects Committee at the National Cerebral and Cardiovascular Center. Nine Japanese white rabbits weighing 2.3 kg to 3.0 kg were anesthetized via intravenous administration of pentobarbital sodium (30–35 mg/kg) through a marginal ear vein. A tracheal tube was inserted through a midline cervical incision. The animal was ventilated mechanically with room air mixed with oxygen through the tracheal tube. The anesthesia was maintained using a continuous intravenous infusion of urethane (125 mg/kg h^{-1}) and α-chloralose (20 mg/kg h^{-1}) through a catheter inserted into the right femoral vein. Mean arterial pressure (AP) was measured by a biological amplifier unit 2238 (San-ei, Japan) using a fluid-filled transducer (BD DTXPlus, Becton, Dickinson and Company) connected to a catheter inserted into the right femoral artery. Heart rate (HR) was derived from an electrocardiogram. Through a midline thoracotomy, the right thymus was removed. A main branch of the right cardiac sympathetic nerve was sectioned to reduce a possible

* Corresponding author. Department of Cardiovascular Dynamics, National Cerebral and Cardiovascular Center Research Institute, 5-7-1 Fujishirodai, Suita, Osaka 565-8565, Japan. Tel.: +81 6 6833 5012 x 2427; fax: +81 6 6835 5403.
E-mail address: torukawa@res.ncvc.go.jp (T. Kawada).

1566-0702/$ – see front matter © 2010 Elsevier B.V. All rights reserved.
doi:10.1016/j.autneu.2010.04.003

sympatho-vagal interaction in the ACh release. After incising the pericardium, a dialysis probe was implanted within the right atrial wall near the junction with the superior vena cava where the sinoatrial node resides (Shimizu et al., 2009). Bilateral vagal nerves were exposed and sectioned at the neck. A pair of platinum electrodes was attached to each sectioned nerve to stimulate the efferent vagal nerve. The dialysis probe was examined postmortem to confirm that it did not penetrate into the atrial cavity.

Acetylcholine was measured in the dialysate as an index of interstitial ACh concentrations. A dialysis fiber (outer diameter, 310 μm; inner diameter, 200 μm; PAN-1200, 50,000-Da molecular-weight cutoff, Asahi Chemical, Japan) was glued at both ends to polyethylene tubes (length, 25 cm; outer diameter, 500 μm; inner diameter, 200 μm) (Akiyama et al., 1994, Shimizu et al., 2009). The end of the polyethylene tube was enlarged by a dulled needle so that the dialysis fiber could be inserted. The exposed fiber length was 4 mm. The dialysis probe was perfused at a rate of 2 μl/min with Ringer solution containing a cholinesterase inhibitor eserine (100 μM). The amount of ACh in the dialysate was measured using a high-performance liquid chromatography system with electrochemical detection (Eicom, Japan) adjusted to measure low concentrations of ACh (Shimizu et al., 2009).

Two hours after the probe implantation, 10-minute dialysate samples were collected under control conditions, before and during bilateral vagal stimulation (10 V, 1-ms pulse width, 10 Hz). The actual dialysate sampling lagged behind a given collection period by 5 min taking into account the dead space volume between the dialysis membrane and collecting tube. After collecting the control data, the perfusate was replaced with the one containing iberiotoxin (2 μM). The local iberiotoxin administration (Ib_{Local}) is considered to affect vagal nerve terminals in the vicinity of the dialysis fiber. The dose was 40 times higher than that used in the in vitro experimental settings (Pedarzani et al., 2000), taking into account the distribution across the dialysis fiber. According to a previous study in rats (Akiyama et al., 2010), local administration of iberiotoxin at half dose (1 μM) significantly enhanced presynaptic ACh release in response to splanchnic nerve stimulation. Thirty minutes after the initiation of Ib_{Local}, 10-minute dialysate samples were collected before and during bilateral vagal stimulation. Next, iberiotoxin was administered intravenously (0.11 mg/body or 37–48 μg/kg, bolus) while continuing the local iberiotoxin administration. The dose was determined based on a previous study in rats (Meade, 1998) in which intravenous administration of iberiotoxin at approximately half dose (20 μg/kg) significantly blocked BK channels. The local plus intravenous iberiotoxin administration (Ib_{L+IV}) is considered to affect both preganglionic and postganglionic vagal nerve terminals. Ten minutes later, 10-minute dialysate samples were collected before and during bilateral vagal stimulation.

In order to check that a locally administered agent did not reach the vagal ganglia, a supplemental protocol was performed at the end of the experiment in five out of the nine rabbits as follows. The perfusate was replaced with the one containing a ganglionic blocker hexamethonium bromide (100 μM in one rabbit and 1 mM in four rabbits). Thirty minutes later, 10-minute dialysate samples were collected before and during bilateral vagal stimulation.

All data are presented as mean and SE values. Dialysate ACh concentrations were compared among three conditions of control, Ib_{Local} and Ib_{L+IV}, using the Friedman test based on ranks, followed by the rank-sum version of the Student–Newman–Keuls test for all pairwise comparisons (Glantz, 2002). AP and HR were measured just before and at 5 min of the 10-minute bilateral vagal stimulation. The AP and HR data were compared among the three conditions using repeated-measures analysis of variance followed by the parametric version of the Student–Newman–Keuls test (Glantz, 2002). In all of the statistical analyses, differences were considered significant when $P<0.05$.

3. Results

Baseline ACh measured before vagal stimulation did not differ significantly among the three conditions (Fig. 1A, left). Vagal stimulation-induced ACh release was significantly enhanced during the Ib_{Local} (118 ± 5% of the control) and Ib_{L+IV} conditions (129 ± 8% of the control) (Fig. 1A, right). There was no significant difference in the stimulation-induced ACh recovery between the Ib_{Local} and Ib_{L+IV} conditions.

Baseline HR measured before vagal stimulation did not differ significantly among the three conditions (Fig. 1B, left). The stimulation-induced bradycardia was augmented during the Ib_{L+IV} but not the Ib_{Local} conditions compared to the control conditions (Fig. 1B, right).

Baseline AP measured before vagal stimulation did not differ significantly among the three conditions (Fig. 1C, left). AP during vagal stimulation was significantly higher during the Ib_{L+IV} conditions compared to that under the control or Ib_{Local} conditions (Fig. 1C, right).

In the supplemental protocol of local hexamethonium administration, the ACh concentration was 3.3 ± 1.1 nM before vagal stimulation. Bilateral vagal stimulation increased the ACh levels in all of the 5 rabbits to 10.9 ± 7.3 nM ($P<0.05$, one-tailed signed test).

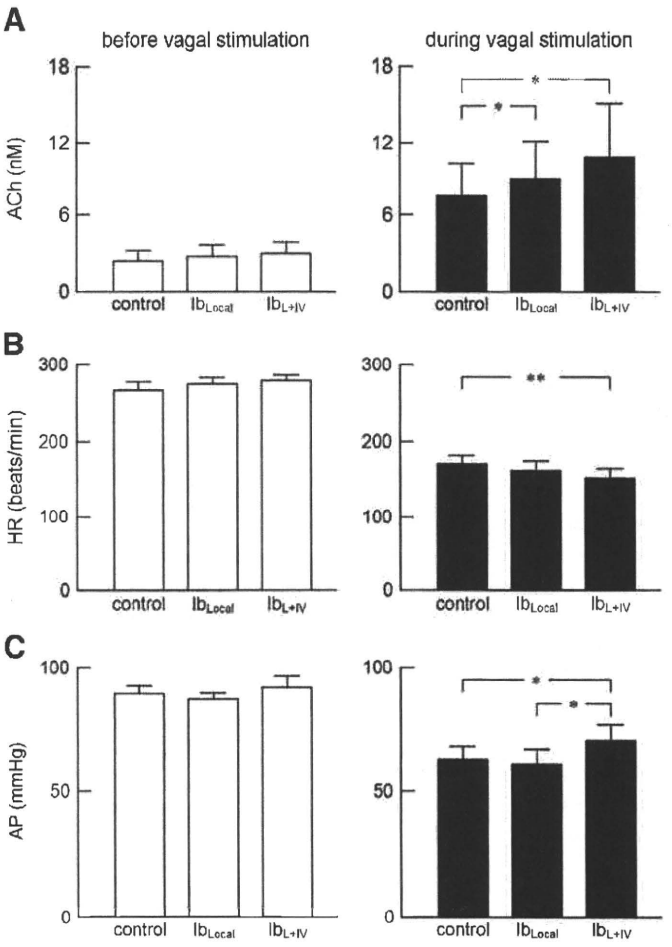

Fig. 1. A: Dialysate acetylcholine (ACh) concentrations under conditions of control, local iberiotoxin administration (Ib_{Local}) and local plus intravenous iberiotoxin administration (Ib_{L+IV}), before (left panel) and during (right panel) bilateral preganglionic vagal stimulation. Ib_{Local} and Ib_{L+IV} significantly increased the vagal stimulation-induced ACh release. B: Heat rate (HR) measured before (left panel) and during (right panel) vagal stimulation. Ib_{L+IV} significantly decreased the HR during vagal stimulation compared to that under control conditions. C: Arterial pressure (AP) measured before (left panel) and during (right panel) vagal stimulation. Ib_{L+IV} significantly increased the AP during vagal stimulation compared to that under the control and Ib_{Local} conditions. Values are mean and mean + SE. $^{*}P<0.05$ and $^{**}P<0.01$.

4. Discussion

Ib_{Local} significantly increased the vagal stimulation-induced ACh release, suggesting that the BK channels play an inhibitory role in the efferent cardiac vagal system (Fig. 1A, right). In a previous study, intravenous administration of hexamethonium bromide completely blocked the vagal stimulation-induced ACh release (Shimizu et al., 2009). In the present study, locally administered hexamethonium bromide is considered to have spread beyond the distribution of locally administered iberiotoxin because of the higher concentration (100 μM or 1 mM vs. 2 μM) and the smaller molecular weight (362.2 vs. 4232.0). Nevertheless, the locally administered hexamethonium bromide did not block the vagal stimulation-induced ACh release, suggesting that the locally administered pharmacological agents failed to reach the vagal ganglia. Therefore, the enhancement of the vagal stimulation-induced ACh release by Ib_{Local} may be attributable to the blockade of the BK channels at the postganglionic vagal nerve terminals.

Under experimental settings similar to the present study, the ACh release at the sinoatrial node can be increased more than 7 times higher during 40-Hz vagal stimulation than during 10-Hz vagal stimulation (Shimizu et al., 2009), suggesting that there remained a sufficient margin for the postganglionic vagal nerve to increase its activity to release ACh when the preganglionic vagal nerve was stimulated at 10 Hz. Under the Ib_{L+IV} conditions, the BK channels are assumed to be blocked at both the preganglionic and postganglionic vagal nerve terminals. If the BK channels limited the preganglionic ACh release to a considerable extent, Ib_{L+IV} could increase the postganglionic vagal nerve activity in response to the preganglionic vagal nerve stimulation. The stimulation-induced ACh release, however, did not differ statistically between the Ib_{Local} and Ib_{L+IV} conditions, suggesting that the inhibitory role of the BK channels at the preganglionic vagal nerve terminals, if any, did not surpass that at the postganglionic vagal nerve terminals.

Although vagi were sectioned at the neck, ACh was detected before vagal stimulation (Fig. 1A, left). In contrast to the vagal stimulation-induced ACh release, the basal ACh release was not affected significantly by Ib_{Local} or Ib_{L+IV}. According to a study using the isolated rat atrium (Abramochkin et al., 2010), a non-quantal ACh release, probably via the choline uptake system, contributes to the basal ACh release from the vagal nerve terminals. It is likely that the blockade of BK channels did not affect the baseline ACh concentrations significantly because the voltage-dependent Ca^{2+} channels contributed little to the basal ACh release.

HR during vagal stimulation under the Ib_{Local} conditions did not differ significantly from that observed under the control conditions (Fig. 1B, right). Presuming that Ib_{Local} affected the ACh release only in the vicinity of the dialysis fiber, not all the vagal nerve fibers innervating the sinoatrial node might have been affected by iberiotoxin. In contrast, HR during vagal stimulation under the Ib_{L+IV} conditions was significantly lower than that observed under the control conditions, suggesting perhaps that the systemically administered iberiotoxin reached a larger portion of the vagal fibers innervating the sinoatrial node.

Ib_{Local} did not affect AP both before and during vagal stimulation (Fig. 1C). Ib_{L+IV} did not increase AP but reduced the vagally mediated hypotension. Possible explanation is as follows. Vagal stimulation significantly decreased AP, possibly via the suppression of cardiac function. Resultantly, the systemic sympathetic system might have been activated through the arterial baroreflex during vagal stimulation. Blockade of the BK channels enhances the vasoconstriction of vascular smooth muscles (Ledoux et al., 2006) and the catecholamine release from the adrenal medulla (Akiyama et al., 2010), resulting in the higher AP during vagal stimulation under the Ib_{L+IV} conditions. The moderation of the vagally mediated hypotension may also have resulted from a more efficient baroreflex response under the Ib_{L+IV} conditions.

There are several limitations in the present study. First, eserine was added to the perfusate to improve the recovery of ACh. Although the inhibition of cholinesterase activity may have affected the ACh kinetics, its influence should have been consistent throughout the protocols. Second, vagal stimulation intensity was selected to limit the hypotensive response and maintain the AP at 60 mm Hg or higher under the control conditions. Based on the results of unilateral vagal stimulation in a previous study (Shimizu et al., 2009), increasing the stimulation frequency would further increase the ACh release. The inhibitory effects of the BK channels on the efferent cardiac vagal system could be different under such an intense vagal stimulation. Finally, the present results do not preclude that the BK channels are on the post-junctional sinus nodal cells or on the cross-inhibitory adrenergic nerves. Nevertheless, the BK channels on the sinus nodal cells or on the adrenergic nerves do not well account for the present results as follows. Although the BK channels on the sinus nodal cells may have modified the HR response and caused possible dissociation between the ACh recovery and the degree of bradycardia, they may not explain the enhanced ACh recovery after the iberiotoxin administration. With respect to the BK channels on the cross-inhibitory adrenergic nerves, if the BK channels are inhibitory to catecholamine release, iberiotoxin is expected to enhance the catecholamine release, antagonizing rather than promoting the vagal ACh release during vagal stimulation. Further studies are needed to confirm these speculations.

In conclusion, blockade of the BK channels by iberiotoxin enhanced the vagal stimulation-induced ACh release and bradycardia, suggesting an inhibitory role of the BK channels in the efferent cardiac vagal system. The inhibitory role of the BK channels at the vagal ganglia did not seem to surpass that at the postganglionic vagal nerve terminals. Although a potential use of selective BK channel openers is expected as vasodilators for vascular smooth muscle dysfunction (Ledoux et al., 2006), there is a possibility that BK channel openers limit vagal effect on the heart, which can be undesirable in certain cardiovascular diseases in which improved vagal function would be helpful.

Acknowledgments

This study was supported by Health and Labour Sciences Research Grants (H18-nano-Ippan-003, H19-nano-Ippan-009, H20-katsudo-Shitei-007, and H21-nano-Ippan-005) from the Ministry of Health, Labour and Welfare of Japan; by a Grant-in-Aid for Scientific Research (No. 20390462) from the Ministry of Education, Culture, Sports, Science and Technology of Japan; and by the Industrial Technology Research Grant Program from the New Energy and Industrial Technology Development Organization (NEDO) of Japan.

References

Abramochkin, D.V., Nurullin, L.F., Borodinova, A.A., Tarasova, N.V., Sukhova, G.S., Nikolsky, E.E., Rosenshtraukh, L.V., 2010. Non-quantal release of acetylcholine from parasympathetic nerve terminals in the right atrium of rats. Exp. Physiol. 95 (2), 265–273.

Akiyama, T., Yamazaki, T., Kawada, T., Shimizu, S., Sugimachi, M., Shirai, M., 2010. Role of Ca^{2+}-activated K^+ channels in catecholamine release from in vivo rat adrenal medulla. Neurochem. Int. 56, 263–269.

Akiyama, T., Yamazaki, T., Ninomiya, I., 1994. In vivo detection of endogenous acetylcholine release in cat ventricles. Am. J. Physiol. 266 (3 Pt 2), H854–H860.

Glantz, S.A., 2002. Primer of Biostatistics, 5th ed. McGraw-Hill, New York.

Ledoux, J., Werner, M.E., Brayden, J.E., Nelson, M.T., 2006. Calcium-activated potassium channels and the regulation of vascular tone. Physiol. 21, 69–79.

Meade, C.J., 1998. The mechanism by which epinastine stops an adenosine analog from contracting BDE rat airways. Am. J. Respir. Crit. Care Med. 157, 522–530.

Pedarzani, P., Kulik, A., Müller, M., Ballanyi, K., Stocker, M., 2000. Molecular determinants of Ca^{2+}-dependent K^+ channel function in rat dorsal vagal neurones. J. Physiol. 527, 283–290.

Shimizu, S., Akiyama, T., Kawada, T., Shishido, T., Yamazaki, T., Kamiya, A., Mizuno, M., Sano, S., Sugimachi, M., 2009. In vivo direct monitoring of vagal acetylcholine release to the sinoatrial node. Auton. Neurosci. 148, 44–49.

Experimental Physiology – *Research Paper*

Dynamic characteristics of heart rate control by the autonomic nervous system in rats

Masaki Mizuno[1,2], Toru Kawada[2], Atsunori Kamiya[2], Tadayoshi Miyamoto[2,3], Shuji Shimizu[2], Toshiaki Shishido[2], Scott A. Smith[1] and Masaru Sugimachi[2]

[1]*Departments of Physical Therapy and Internal Medicine, University of Texas Southwestern Medical Center at Dallas, TX, USA*
[2]*Department of Cardiovascular Dynamics, National Cerebral and Cardiovascular Center Research Institute, Osaka, Japan*
[3]*Department of Physical Therapy, Morinomiya University of Medical Sciences, Osaka, Japan*

We estimated the transfer function of autonomic heart rate (HR) control by using random binary sympathetic or vagal nerve stimulation in anaesthetized rats. The transfer function from sympathetic stimulation to HR response approximated a second-order, low-pass filter with a lag time (gain, 4.29 ± 1.55 beats min^{-1} Hz^{-1}; natural frequency, 0.07 ± 0.03 Hz; damping coefficient, 1.96 ± 0.64; and lag time, 0.73 ± 0.12 s). The transfer function from vagal stimulation to HR response approximated a first-order, low-pass filter with a lag time (gain, 8.84 ± 4.51 beats min^{-1} Hz^{-1}; corner frequency, 0.12 ± 0.06 Hz; and lag time, 0.12 ± 0.08 s). These results suggest that the dynamic characteristics of HR control by the autonomic nervous system in rats are similar to those of larger mammals.

(Received 5 March 2010; accepted after revision 24 May 2010; first published online 28 May 2010)
Corresponding author M. Mizuno: Department of Physical Therapy, University of Texas Southwestern Medical Center at Dallas, 5323 Harry Hines Boulevard, Dallas, TX 75390-9174, USA. Email: masaki.mizuno@utsouthwestern.edu

Despite extensive use of rats in cardiovascular research, the dynamic characteristics of heart rate (HR) control by the autonomic nervous system in this species remain to be elucidated. To better understand the autonomic control of HR in rats, it is important to quantitatively assess the input–output relationship between autonomic nerve stimulation and HR over a wide range of frequencies that are of physiological interest. By understanding these relationships in the rat, data obtained using this animal model may be more readily extrapolated to larger mammals, including humans.

Heart rate variability is considered to reflect autonomic tone because its components change both physiologically (e.g. standing and ageing) and pathophysiologically (e.g. hypertension and heart failure; Malliani *et al.* 1991). Based on dog and human studies, the very low-frequency (VLF) component (0.02–0.08 Hz) is likely to reflect changes in vasomotor tone in relation to thermoregulation and local adjustment of resistance in individual vascular beds; the low-frequency (LF) component (0.08–0.15 Hz) is considered to be Mayer's wave and a marker of sympathetic activity; and the high-frequency (HF) component (0.15–0.40 Hz) mainly originates from respiratory activity and is considered to be mediated by vagal activity (Pagani *et al.* 1986). Based on the differences in HR spectra between conscious rats and rats in which autonomic blockade was induced pharmacologically, Cerutti *et al.* (1991) determined that the VLF component ranged between 0.017 and 0.26 Hz, the LF component ranged between 0.27 and 0.74 Hz, and the HF component was above 0.75 Hz. Even though these allocations in frequency band in rats corresponded to their considerably higher basal HR (range between 300 and 400 beats min^{-1}) compared with that of larger mammals, such as dogs and humans (range between 60 and 100 beats min^{-1}), there has been no scientific rationale provided for setting these allocations. This is because it is unknown whether the dynamic characteristics of HR control by the autonomic nervous system in rats are significantly different from those in larger mammals, such as rabbits (Kawada *et al.* 1996), cats (Chess & Calaresu, 1971) and dogs (Berger *et al.* 1989).

Given that the release and disposition of neurotransmitters (e.g. noradrenaline and acetylcholine) at autonomic nerve endings may be determined biochemically, regardless of body size, we hypothesized that the dynamic characteristics of HR control by the autonomic nervous system would not differ appreciably among different mammalian species. To test this

DOI: 10.1113/expphysiol.2010.053090

hypothesis, we quantified the dynamic characteristics of HR control mediated by sympathetic or vagal nerve stimulation in rats using transfer function analysis. The results provide the first quantitative data on the dynamic characteristics of autonomic HR regulation in rats. Since HR changes dynamically in response to daily activities, quantification of how quickly the HR can respond to sympathetic or vagal nerve stimulation is important. For instance, information on the dynamic HR response is key to understanding the generation of HR variability. The present study aims to expand our knowledge of HR control by the autonomic nervous system.

Methods

Surgical preparation

Animal care was in accordance with the *Guiding Principles for Care and Use of Animals in the Field of Physiological Sciences*, approved by the Physiological Society of Japan. All protocols were reviewed and approved by the Animal Subjects Committee of the National Cerebral and Cardiovascular Center. Thirteen Sprague–Dawley rats (body weight, 340–670 g) were anaesthetized using a mixture of urethane (250 mg ml^{-1}; Sigma, St. Louis, MO, USA) and α-chloralose (40 mg ml^{-1}; Sigma), initiated with an intraperitoneal bolus injection of 1 ml kg^{-1}. If additional anaesthesia was needed, 0.1 ml kg^{-1} was given intraperitoneally. The rats were intubated and mechanically ventilated with oxygen-enriched room air. The rats were slightly hyperventilated to suppress chemoreflexes (arterial P_{CO_2} ranged from 30 to 35 mmHg; arterial P_{O_2} > 300 mmHg). Arterial blood pH was within the physiological range. A catheter was placed in the right femoral artery, which was connected to a pressure transducer (DX-200, Nihon Kohden, Tokyo, Japan) to measure arterial pressure (AP). Heart rate was measured using a cardiotachometer (AT601G, Nihon Kohden, Tokyo, Japan) triggered by the R wave on the electrocardiogram. The HR series were checked by visual inspection. A catheter was introduced into the right femoral vein for drug administration. Sino-aortic denervation was performed bilaterally to minimize changes in the sympathetic efferent nerve activity via arterial baroreflexes. The vagi were sectioned bilaterally at the neck. A pair of bipolar stainless-steel electrodes was attached to the right cervical sympathetic nerve for efferent sympathetic stimulation or the right cervical vagus for efferent vagal stimulation. The stimulation electrodes and nerve were secured with silicon glue (Kwik-Sil, World Precision Instruments, Sarasota, FL, USA). Body temperature was monitored with a thermometer placed in the rectum, and was maintained at 38°C with a heating pad throughout the experiment.

Experimental procedures

The pulse duration was set at 2 ms and the stimulation amplitude was fixed at 10 V for both sympathetic and vagal nerve stimulation. To allow stable haemodynamics, sympathetic and vagal nerve stimulation was started at ~1 h after the end of surgical preparation. Between sympathetic and vagal stimulation protocols, >15 min elapsed to allow AP and HR to return to their respective baseline values.

To estimate the dynamic transfer characteristics from sympathetic stimulation to the HR response, the sectioned end of the right cervical sympathetic nerve was stimulated, employing a frequency-modulated pulse train for 10 min. The stimulation frequency was switched every 1000 ms to either 0 or 5 Hz, according to a binary white-noise signal. The power spectrum of the stimulation signal was reasonably constant up to 0.5 Hz. The transfer function was estimated up to 0.5 Hz because the reliability of estimation decreased owing to the diminution of input power above this frequency. The selected frequency range was determined based on previous results in rabbits (Kawada *et al.* 1996) so that it would sufficiently span the physiological range of interest with respect to the dynamic sympathetic control of HR.

To estimate the dynamic transfer characteristics from vagal stimulation to the HR response, the right vagus was stimulated, employing a frequency-modulated pulse train for 10 min. The stimulation frequency was switched every 500 ms to either 0 or 10 Hz, according to a binary white-noise signal. The power spectrum of the stimulation signal was reasonably constant up to 1 Hz. The transfer function was estimated up to 1 Hz because the reliability of estimation decreased owing to the diminution of input power above this frequency. The selected frequency range was determined based on previous results in rabbits (Kawada *et al.* 1996) so that it would sufficiently span the physiological range of interest with respect to the dynamic vagal control of HR.

The switching intervals differed between sympathetic and vagal stimulation for the following reasons. In theory, the switching interval of binary white noise is inversely related to an upper frequency bound for the input modulation frequency. Prior knowledge in rabbits (Kawada *et al.* 1996) and preliminary results in rats indicated that the upper frequency bound of physiological interest might be lower for the sympathetic transfer function, which rendered the switching interval longer for the sympathetic stimulation. Another reason relates to the stimulation frequency. In the present study, the sympathetic stimulation frequency of 5 Hz and the vagal stimulation frequency of 10 Hz were determined based on the HR response. Once the stimulation frequency is determined, there is a methodological limitation for setting the switching interval. For example, a switching

interval of 500 ms is too close to a pulse interval of 200 ms (i.e. 5 Hz stimulation). In this case, only two pulses can be applied in the shortest interval of 500 ms, which means that the stimulation frequency may be in effect 4 Hz rather than the intended 5 Hz. This problem does not occur with a 1000 ms switching interval in combination with 5 Hz stimulation and 500 ms switching interval in combination with 10 Hz stimulation.

Background sympathetic tone is known to augment vagal HR control (an accentuated antagonism; Levy, 1971; Kawada *et al.* 1996). To eliminate any effect of sympathetic activity, in seven out of the thirteen rats the vagal stimulation protocol was repeated after the administration of the β-adrenergic blocker propranolol (1 mg kg^{-1} I.V.; Perlini *et al.* 1995).

Data analysis

Data were digitized at 200 Hz using a 12 bit analog-to-digital converter and stored on the hard disk of a dedicated laboratory computer system. The dynamic transfer function from binary white-noise stimulation to the HR response was estimated based on the following procedure. To avoid the possibility that the initial transition from no stimulation to random stimulation biased the transfer function estimation, data were processed only from 2 min after the initiation of random stimulation. Input–output data pairs of the stimulation frequency and HR were resampled at 10 Hz. Subsequently, data pairs were partitioned into eight 50%-overlapping segments consisting of 1024 data points each. For each segment, the linear trend was subtracted and a Hanning window was applied. A fast Fourier transform was then performed to obtain the frequency spectra of nerve stimulation [$N(f)$] and HR [$HR(f)$]. Over the eight segments, the power of the nerve stimulation [$S_{N\cdot N}(f)$], the power of the HR [$S_{HR\cdot HR}(f)$], and the cross-power between these two signals [$S_{N\cdot HR}(f)$] were ensemble averaged. Finally, the transfer function [$\mathrm{H}(f)$] from nerve stimulation to the HR response was determined using the following equation (Marmarelis & Marmarelis, 1978):

$$\mathrm{H}(f) = \frac{S_{N\cdot HR}(f)}{S_{N\cdot N}(f)} \quad (1)$$

To quantify the linear dependence of the HR response on vagal or sympathetic stimulation, the magnitude-squared coherence function [$\mathrm{Coh}(f)$] was estimated by employing the following equation (Marmarelis & Marmarelis, 1978):

$$\mathrm{Coh}(f) = \frac{|S_{N\cdot HR}(f)|^2}{S_{N\cdot N}(f) \times S_{HR\cdot HR}(f)} \quad (2)$$

Coherence values range from zero to unity. Unity coherence indicates perfect linear dependence between the input and output signals; in contrast, zero coherence indicates total independence between the two signals.

As preliminary results suggested that the transfer function from sympathetic stimulation to HR response in rats approximated a second-order low-pass filter with pure delay, as in the case of rabbits (Kawada *et al.* 1996, 2009), we determined the parameters of the sympathetic transfer function using the following equation:

$$\mathrm{H}(f) = \frac{K}{1 + 2\zeta\frac{f}{f_\mathrm{N}}j + \left(\frac{f}{f_\mathrm{N}}j\right)^2} \mathrm{e}^{-2\pi f j L} \quad (3)$$

where K is dynamic gain (in beats per minute per herz), f_N is the natural frequency (in herz), ζ is the damping ratio, L is lag time (in seconds), and f and j represent frequency and imaginary units, respectively. The dynamic gain (K, in beats per minute per herz) represents the asymptotic value of transfer gain as the frequency approaches zero, and corresponds to the steady-state response in the step response. The natural frequency (f_N, in herz) determines the frequency limit of the low-pass filter above which the transfer gain reduces as the frequency increases. In the second-order low-pass filter, the maximal negative slope of the gain diminution is 1/100 per 10 Hz. The damping ratio (ζ, unitless) characterizes how the transfer gain varies around the f_N. The lag time (L, in seconds) indicates the latency of signal transmission from nerve stimulation to the initiation of HR response. These parameters were estimated by means of an iterative non-linear least-squares regression.

As preliminary results suggested that the transfer function from vagal stimulation to HR response in rats approximated a first-order low-pass filter with pure delay, as in the case of rabbits (Kawada *et al.* 1996, 2009), we determined the parameters of the vagal transfer function using the following equation:

$$\mathrm{H}(f) = \frac{-K}{1 + \frac{f}{fc}j} \mathrm{e}^{-2\pi f j L} \quad (4)$$

where K represents the dynamic gain (in beats per minute per herz), fc denotes the corner frequency (in herz), L denotes the lag time (in seconds), and f and j represent frequency and imaginary units, respectively. The negative sign in the numerator indicates the negative HR response to vagal stimulation. The dynamic gain (K, in beats per minute per herz) represents the asymptotic value of transfer gain as the frequency approaches zero. The corner frequency (fc, in herz) represents the frequency at which the transfer gain decreases by 3 dB relative to K. Higher fc indicates the more rapid HR response to vagal stimulation. In the first-order low-pass filter, the maximal slope of the gain diminution is 1/10 per 10 Hz. The lag time (L, in seconds) indicates the latency of signal transmission from nerve stimulation to the initiation of HR response. These

parameters were estimated by means of an iterative non-linear least-squares regression.

To facilitate the intuitive understanding of the system's dynamic characteristics, we calculated the system step response of HR to 1 Hz nerve stimulation as follows. The system impulse response was derived from the inverse Fourier transform of $H(f)$. The system step response was then obtained from the time integral of the impulse response. The length of the step response was 51.2 s. The 80% rise time for sympathetic step response or the 80% fall time for vagal step response was estimated at the time which the step response reached 80% of the steady-state response, calculated by averaging the last 10 s of data from the step response.

Statistical analysis

All data are represented as means ± S.D. Student's paired *t* test was used to test differences in haemodynamic parameters. In seven rats, parameters of vagal transfer function were compared before and after propranolol administration using Student's paired *t* test. Values of $P < 0.05$ were considered significant.

Results

Typical recordings

Figure 1 shows typical recordings of sympathetic and vagal stimulation obtained from one rat. While HR varied immediately during random vagal stimulation, it changed only gradually during random sympathetic stimulation. Sympathetic stimulation increased the mean HR from 375.5 ± 33.5 to 444.9 ± 28.4 beats min^{-1} ($P < 0.05$); vagal stimulation decreased the mean HR from 378.2 ± 31.9 to 317.3 ± 47.1 beats min^{-1} ($P < 0.05$). Neither sympathetic nor vagal stimulation altered mean AP (79.1 ± 18.4 *versus* 75.1 ± 19.4 and 78.2 ± 20.2 *versus* 72.4 ± 18.3 mmHg, respectively).

Sympathetic transfer function

Figure 2*A* illustrates the dynamic transfer function characterizing sympathetic HR control averaged from all animals. Gain plots, phase plots and coherence functions are shown. The sympathetic transfer function approximated a second-order, low-pass filter with a lag time (dynamic gain, 4.29 ± 1.55 beats min^{-1} Hz^{-1}; natural frequency, 0.07 ± 0.03 Hz; damping coefficient, 1.96 ± 0.64; and lag time, 0.73 ± 0.12 s). Figure 2*B* shows the calculated step response of HR to sympathetic stimulation averaged from all animals. As expected, sympathetic stimulation gradually increased HR. The steady-state sympathetic response was 3.86 ± 1.80 beats min^{-1} Hz^{-1}. The 80% rise time for the sympathetic step response was 13.7 ± 5.1 s.

Vagal transfer function

Figure 2*C* illustrates the dynamic transfer function characterizing vagal HR control averaged from all animals. The vagal transfer function approximated a first-order, low-pass filter with a lag time (dynamic gain, 8.84 ± 4.51 beats min^{-1} Hz^{-1}; corner frequency, 0.12 ± 0.06 Hz; and lag time, 0.12 ± 0.08 s). Figure 2*D* shows the calculated step response of HR to vagal

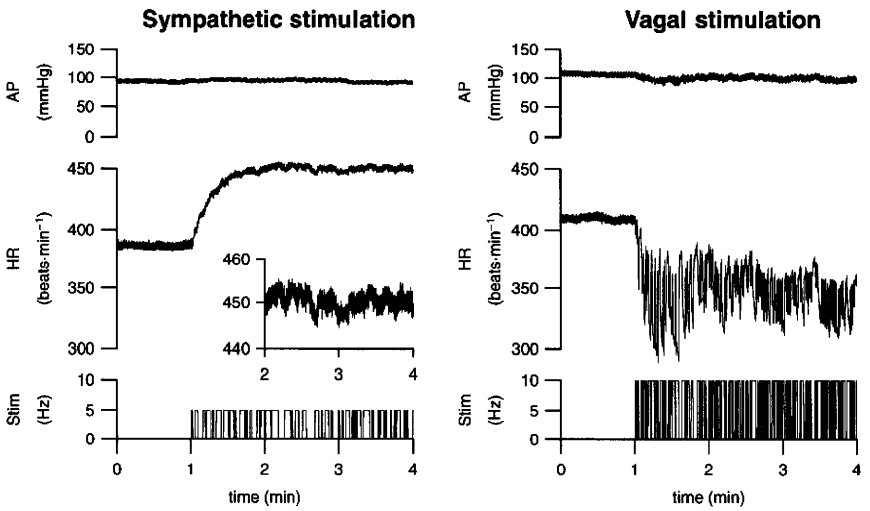

Figure 1. Raw trace of 10 Hz resampled arterial pressure (AP; top) and heart rate (HR; middle) obtained using binary white-noise stimulation (Stim; bottom)
Recordings are shown for sympathetic (left) and vagal nerve stimulation (right). The inset in the panels for sympathetic stimulation indicates the expanded ordinate for the HR response.

stimulation averaged from all animals. As expected, vagal stimulation decreased HR. The vagal HR response appeared more quickly than the sympathetic HR response. The steady-state vagal response was 9.63 ± 5.21 beats min^{-1} Hz^{-1}. The 80% fall time for the vagal step response was 4.13 ± 1.74 s.

β-Adrenergic blockade did not significantly affect any parameters of the vagal transfer function (dynamic gain, 7.96 ± 2.97 *versus* 7.75 ± 2.49 beats min^{-1} Hz^{-1}; corner frequency, 0.12 ± 0.05 *versus* 0.11 ± 0.05 Hz; and lag time, 0.10 ± 0.08 *versus* 0.17 ± 0.08 s, before and after β-adrenergic blockade, respectively).

Discussion

We have demonstrated the first quantitative data on the dynamic characteristics of HR control by the sympathetic and vagal nerves in rats. These results suggest that the dynamic characteristics of autonomic HR control in rats are similar to those of larger mammals despite basal HR being higher in these animals.

Sympathetic transfer function

In the present study, we stimulated the preganglionic cardiac sympathetic nerve instead of the postganglionic cardiac sympathetic nerve because of technical reasons. Therefore, the sympathetic transfer function was estimated from the combined dynamic characteristics of ganglionic and postganglionic transmission. Nevertheless, the sympathetic transfer function approximated a second-order delay system (Fig. 2*A*) and its parameters were similar to those estimated between postganglionic sympathetic stimulation and HR response in rabbits

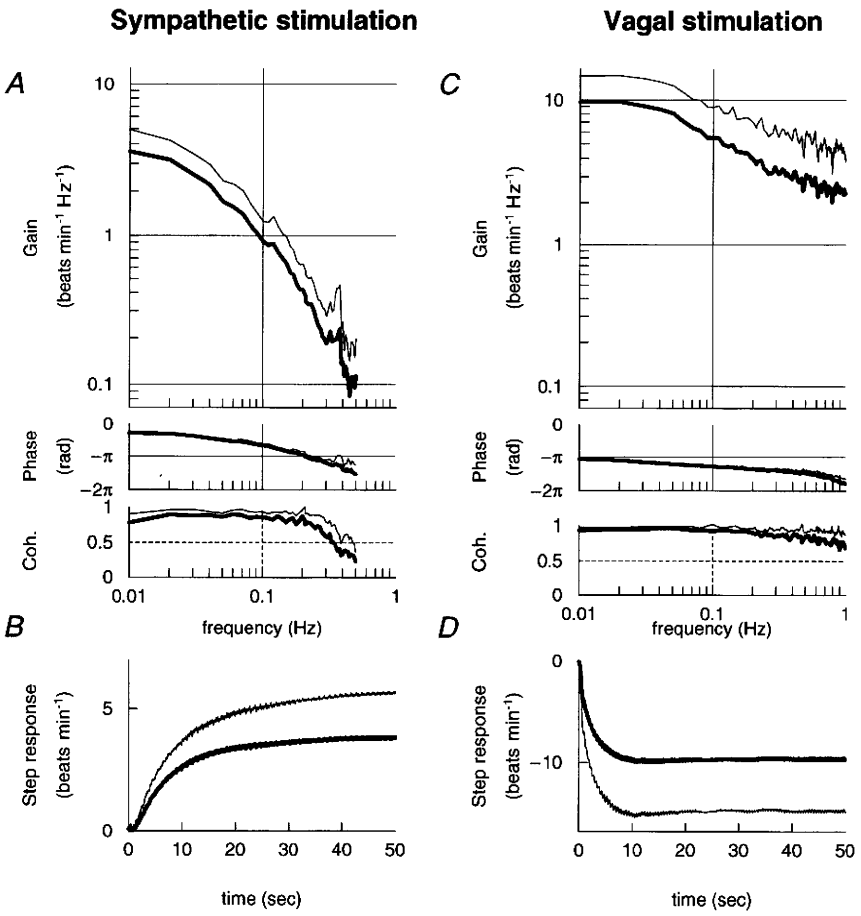

Figure 2. Transfer functions and step responses of HR to sympathetic and vagal stimulation
A, dynamic transfer function relating sympathetic stimulation to the HR response averaged from all animals. Gains (top), phase shifts (middle) and coherence functions (bottom) are presented. *B*, calculated step response to 1 Hz tonic sympathetic stimulation averaged from all animals. *C*, dynamic transfer function relating vagal stimulation to the HR response averaged from all animals. Gains (top), phase shifts (middle) and coherence functions (bottom) are presented. *D*, calculated step response to 1 Hz tonic vagal stimulation averaged from all animals. Thick lines represent the mean, whereas thin lines indicate + S.D. values.

(natural frequency, 0.06–0.07 Hz; damping coefficient, 1.34–1.53; and lag time, 0.51–0.65 s; Kawada *et al.* 2009). If we calculate the corner frequency (frequency at which gain decreased by 3 dB from steady-state gain; 0.04 ± 0.01 Hz) instead of natural frequency, our results are comparable to the corner frequency (0.01–0.02 Hz) found by Berger *et al.* (1989) using dogs. Thus, in the present study sympathetic transfer function in rats resembles that of dogs. The 80% rise time for sympathetic step response is also comparable to that of rabbits (14.4–17.2 s) as reported by Kawada *et al.* (2009). Therefore, we contend that the dynamic characteristics in ganglionic transmission contribute little to the determination of the overall low-pass characteristics of sympathetic HR control.

Vagal transfer function

The transfer function of vagal stimulation to HR response can be characterized as a first-order delay system (Fig. 2*C*), as in previous reports using rabbits (Kawada *et al.* 1996), dogs (Berger *et al.* 1989) and cats (Chess & Calaresu, 1971). The estimated corner frequency of the transfer function from vagal stimulation to HR response in the present study (0.12 ± 0.06 Hz) is different but of the same order as that of rabbits (0.39 Hz; Kawada *et al.* 2009) and cats (0.05 Hz; Chess & Calaresu, 1971). However, if we calculate the corner frequency as the frequency at which gain decreases by 3 dB from steady-state gain, the value is 0.06 ± 0.01 Hz. Furthermore, the 80% fall time for the vagal step response in rats is also greater than that in rabbits (1.3 s; Kawada *et al.* 2009). Hence, the first-order low-pass filter may not be the best approximation of the transfer function from vagal stimulation to HR response in rats, in contrast to the case in rabbits (Kawada *et al.* 1996, 2009) Furthermore, Berger *et al.* (1989) demonstrated that the effective filter characteristics of the system depend on the mean level of stimulatory rates. Additional studies are needed to clarify some of the disparity in results between the present investigation and other reports. Overall, however, the dynamic transfer function characteristics of HR regulation by the vagus were not appreciably different in rats compared with larger mammals.

Although sino-aortic denervation should have minimized the baroreflex-mediated changes in sympathetic nerve activity, this procedure does not necessarily eliminate the background sympathetic tone. It should be noted that tonic sympathetic stimulation may increase the dynamic gain of the vagal transfer function via accentuated antagonism (Kawada *et al.* 1996). The results of propranolol administration indicated that the effects of background sympathetic tone on the dynamic vagal control of HR were insignificant in the present study.

Physiological implications and perspectives

As mentioned in the Introduction, the allocations in frequency band of HR variability in rats (Cerutti *et al.* 1991) are set in a higher frequency band compared with those of larger mammals, such as dogs and humans (Malliani *et al.* 1991). However, parameters of dynamic characteristics in HR control by the autonomic nervous system in rats were not much different from those reported in larger mammals, suggesting the importance of biochemical processes of neurotransmitter release and disposition in determining dynamic HR response. Therefore, the allocations of HR variability in the HF component in rats may not readily be explained in terms of the dynamic characteristics of HR response to sympathetic and vagal nerve stimulation. Nevertheless, the fact that the vagal HR control is much faster than the sympathetic HR control may contribute to the generation of frequency dependence of HR variability.

To simply identify the dynamic characteristics of HR control by the autonomic nervous system in rats, the present study used Sprague–Dawley rats as normal animals. It has been well documented that exercise training results in increased vagal tone (Coote, 2010) and that pathophysiological conditions, such as chronic heart failure and hypertension, result in increased basal sympathetic tone (Billman, 2009) compared with the normal conditions. Further investigations are needed to clarify the impacts of such physiological and pathophysiological conditions on dynamic characteristics of HR control by the autonomic nervous system in rats.

The absolute gain values of the vagal transfer function seem higher than those previously reported in rabbits (Kawada *et al.* 1996, 2009). In those previous studies, the amplitude of vagal stimulation was adjusted in each animal so that HR was decreased by approximately 50 beats min^{-1} with 5 Hz tonic vagal stimulation. As a result, the stimulation amplitude was below 10 V. In the present study, however, the stimulation amplitude was fixed at 10 V, which would partly account for the larger gain values in the vagal transfer function. The absolute gain values are also affected by the operating HR. When the operating HR is within the saturation range of the HR response, the absolute gain values should be attenuated (Kawada *et al.* 1996). In addition, the magnitude of transfer gain is dependent on a mean stimulation frequency (Berger *et al.* 1989). Accordingly, direct comparison of the absolute gain values among different studies may be difficult based on the currently available data alone.

Limitations

There are several limitations to this study. First, data were obtained from anaesthetized animals. Since anaesthesia affects autonomic tone, the results may not be directly

applicable to conscious animals. Second, we stimulated the autonomic nerve according to binary white noise, which was quite different from the pattern of physiological neuronal discharge. However, the fact that coherence was near unity over the frequency range of interest indicates that, by virtue of their inherent linearity, the system properties would not vary much with differing patterns of stimulation. Finally, we measured AP using a femoral catheter connected to a fluid-filled pressure transducer. Although the computation of the mean pressure might be adequate, a reliable measurement of systolic/diastolic pressure would be difficult in the present study.

Conclusion

In the present study, it was demonstrated for the first time in rats that the transfer function from sympathetic stimulation to HR response approximated a second-order, low-pass filter with a lag time and that from vagal stimulation to HR response approximated a first-order, low-pass filter with a lag time. Despite the large difference in baseline HR, parameters of dynamic characteristics in HR control by the autonomic nervous system in rats are not much different from those reported in larger mammals. As such, the rat can be used as a reliable model for the determination of these parameters.

References

Berger RD, Saul JP & Cohen RJ (1989). Transfer function analysis of autonomic regulation. I. Canine atrial rate response. *Am J Physiol Heart Circ Physiol* **256**, H142–H152.

Billman GE (2009). Cardiac autonomic neural remodeling and susceptibility to sudden cardiac death: effect of endurance exercise training. *Am J Physiol Heart Circ Physiol* **297**, H1171–H1193.

Cerutti C, Gustin MP, Paultre CZ, Lo M, Julien C, Vincent M & Sassard J (1991). Autonomic nervous system and cardiovascular variability in rats: a spectral analysis approach. *Am J Physiol Heart Circ Physiol* **261**, H1292–H1299.

Chess GF & Calaresu FR (1971). Frequency response model of vagal control of heart rate in the cat. *Am J Physiol* **220**, 554–557.

Coote JH (2010). Recovery of heart rate following intense dynamic exercise. *Exp Physiol* **95**, 431–440.

Kawada T, Ikeda Y, Sugimachi M, Shishido T, Kawaguchi O, Yamazaki T, Alexander J Jr & Sunagawa K (1996). Bidirectional augmentation of heart rate regulation by autonomic nervous system in rabbits. *Am J Physiol Heart Circ Physiol* **271**, H288–H295.

Kawada T, Mizuno M, Shimizu S, Uemura K, Kamiya A & Sugimachi M (2009). Angiotensin II disproportionally attenuates dynamic vagal and sympathetic heart rate controls. *Am J Physiol Heart Circ Physiol* **296**, H1666–H1674.

Levy MN (1971). Sympathetic-parasympathetic interactions in the heart. *Circ Res* **29**, 437–445.

Malliani A, Pagani M, Lombardi F & Cerutti S (1991). Cardiovascular neural regulation explored in the frequency domain. *Circulation* **84**, 482–492.

Marmarelis P & Marmarelis V (1978). The white noise method in system identification. In *Analysis of Physiological Systems*, pp. 131–221. Plenum, New York.

Pagani M, Lombardi F, Guzzetti S, Rimoldi O, Furlan R, Pizzinelli P, Sandrone G, Malfatto G, Dell'Orto S, Piccaluga E, Turiel M, Baselli G, Cerutti S & Malliani A (1986). Power spectral analysis of heart rate and arterial pressure variabilities as a marker of sympatho-vagal interaction in man and conscious dog. *Circ Res* **59**, 178–193.

Perlini S, Giangregorio F, Coco M, Radaelli A, Solda PL, Bernardi L & Ferrari AU (1995). Autonomic and ventilatory components of heart rate and blood pressure variability in freely behaving rats. *Am J Physiol Heart Circ Physiol* **269**, H1729–H1734.

Acknowledgements

This study was supported by Health and Labor Sciences Research Grants (H18-nano-Ippan-003, H19-nano-Ippan-009, H20-katsudo-Shitei-007 and H21-nano-Ippan-005) from the Ministry of Health, Labor and Welfare of Japan, by Grants-in-Aid for Scientific Research (no. 19700559) from the Ministry of Education, Culture, Sports, Science and Technology in Japan and by the Industrial Technology Research Grant Program from New Energy and Industrial Technology Development Organization (NEDO) of Japan. M. Mizuno was supported by Research Fellowships of the Japan Society for the Promotion of Science for Young Scientists.

J Physiol Sci (2010) 60:205–212
DOI 10.1007/s12576-010-0086-y

ORIGINAL PAPER

Right ventricular stiffness constant as a predictor of postoperative hemodynamics in patients with hypoplastic right ventricle: a theoretical analysis

Shuji Shimizu · Toshiaki Shishido · Dai Une · Atsunori Kamiya · Toru Kawada · Shunji Sano · Masaru Sugimachi

Received: 9 December 2009 / Accepted: 10 January 2010 / Published online: 4 February 2010

Abstract One and a half ventricle repair (1.5VR) is a surgical option for hypoplastic right ventricle (RV). The benefits of this procedure compared to biventricular repair (2VR) or Fontan operation remain unsettled. To compare postoperative hemodynamics, we performed a theoretical analysis using a computational model based on lumped-parameter state-variable equations. We varied the RV stiffness constant (B_{RV}) to simulate the various RV hypoplasia, and estimated hemodynamics for a given B_{RV}. With $B_{RV} < 150\%$ of normal, cardiac output was the largest in 2VR. With $B_{RV} > 150\%$, cardiac output became larger in 1.5VR than in 2VR. With $B_{RV} > 250\%$, RV end-diastolic volume was almost the same between 1.5VR and 2VR, and a rapid increase in atrial pressure precluded the use of 1.5VR. These results indicate that the beneficial effect of 1.5VR depends on the RV stiffness constant. Determination of management strategy should not only be based on the morphologic parameters but also on the physiological properties of RV.

S. Shimizu (✉) · T. Shishido · D. Une · A. Kamiya · T. Kawada · M. Sugimachi
Department of Cardiovascular Dynamics, Advanced Medical Engineering Center, National Cardiovascular Center Research Institute, 5-7-1 Fujishiro-dai, Suita, Osaka 565-8565, Japan
e-mail: shujismz@ri.ncvc.go.jp

S. Shimizu · S. Sano
Department of Cardiovascular Surgery, Okayama University Graduate School of Medicine, Dentistry and Pharmaceutical Sciences, Okayama, Japan

S. Shimizu
Japan Association for the Advancement of Medical Equipment, Tokyo, Japan

Keywords One and a half ventricle repair · Right ventricular stiffness · Hypoplastic right ventricle · Computational model

Introduction

One and a half ventricle repair (1.5VR) is a surgical option for hypoplastic right ventricle (RV) caused by various congenital heart diseases including pulmonary atresia with intact ventricular septum (PA/IVS), Ebstein's anomaly or their relatives. In this procedure, the superior vena cava (SVC) is directly connected to the pulmonary artery (PA). Therefore, the blood from SVC directly enters PA, whereas the blood from the inferior vena cava (IVC) is pumped by RV to PA. This procedure is clinically acceptable because of its low surgical risk [1, 2]. However, the benefits of this procedure on postoperative hemodynamics in patients with a wide spectrum of RV hypoplasia compared to other procedures such as biventricular repair (2VR) and Fontan operation remain unsettled [3]. Furthermore, conversion to Fontan circulation was required late after 1.5VR in a possibly inappropriate candidate [4].

Although various authors reported an arbitrary selection scheme for the procedures based on RV morphology such as RV end-diastolic volume (RVEDV) [1, 2, 5], the long-term outcomes of 1.5VR have remained insufficiently known [5]. The previous criteria do not likely predict postoperative hemodynamics of these complex circulations accurately because morphological values measured preoperatively largely depend on the RV preload and afterload conditions, which change remarkably between subjects and between before and after the operation.

Hypoplastic RV is physiologically characterized by increased RV stiffness, caused by hypertrophy and

fibroelastosis of RV muscles [6]. However, how RV stiffness influences the postoperative hemodynamics has not been reported. Given the small number of patients with each of the wide variety of preoperative RV conditions [7, 8], the influence of RV stiffness on 1.5VR, 2VR, and Fontan operation cannot be examined by clinical study. It is also difficult to experimentally reproduce hemodynamics before and after 1.5VR for hypoplastic RV with various stiffness. In view of the above, we attempted to clarify postoperative hemodynamics by a theoretical analysis using a computational model based on lumped-parameter state-variable equations. The present results indicate that the RV stiffness constant may provide selection criteria for 1.5VR.

Materials and methods

The electrical analogs of the model used to simulate the cardiovascular system are shown in Fig. 1. We modeled the postoperative cardiovascular system mathematically by a combination of the time-varying elastance cardiac chamber model and the three-element Windkessel vascular model. We set the normal values of parameters to be appropriate for a 75-kg man. These values were obtained from the literature [9–13] and are listed in Table 1. Since the data of the pressure–volume relationship of the atrium were scarcely available, parameters of the atrium were surmised from the literature [10–12].

Heart

The right and left ventricular chambers as well as the atrial chambers are represented by the time-varying elastance model [9, 10, 13]. The end-systolic pressure–volume relationship is described by a linear formula:

$$P_{es,cc} = E_{es,cc}\left[V_{es,cc} - V_{0,cc}\right] \quad (1)$$

where $P_{es,cc}$ and $V_{es,cc}$ are end-systolic pressure and volume, respectively; $E_{es,cc}$ is the maximal volume elastance; $V_{0,cc}$ is the volume at which $P_{es,cc}$ is equal to 0 mmHg. cc denotes each chamber, i.e., RA for the right atrium, LA for the left atrium, RV for the right ventricle, or LV for the left ventricle. The end-diastolic pressure–volume relationship is represented by a non-linear formula:

$$P_{ed,cc} = A_{cc}\left[e^{B_{cc}(V_{ed,cc}-V_{0,cc})} - 1\right] \quad (2)$$

where $P_{ed,cc}$ and $V_{ed,cc}$ are end-diastolic pressure and volume, respectively; A_{cc} and B_{cc} are constants [9, 10, 13]. We assumed the time course of the time-varying elastance by defining normalized elastance curve $e_{cc}(t)$ as:

Table 1 Parameters used in modeling

Heart rate (HR), beats/min	75			
Duration of cardiac cycle (T_c), ms	800			
Time advance of atrial systole (DT), ms	16			
Total stressed blood volume (V_s), ml	750	(control only)		
	LV	RV	LA	RA
Time to end systole (T_{es}), ms	200	200	120	120
End-systolic elastance (E_{es}), mmHg/ml	3.0	0.7	0.5	0.5
Scaling factor of EDPVR (A), mmHg	0.35	0.35	0.06	0.06
Exponent scaling factor for EDPVR (B), ml^{-1}	0.033	0.023	0.264	0.264
Unstressed volume (V_0), ml	0	0	5	5
	Aortic	Pulmonary	Mitral	Tricuspid
Valvular resistance (forward), (mmHg s)/ml	0.001	0.001	0.001	0.001
	Systemic		Pulmonary (p)	
	Superior (ss)	Inferior (si)		
Arterial resistance (R_a), (mmHg s)/ml	2.25	1.5	0.03	
Characteristic impedance (R_c), (mmHg s)/ml	0.075	0.05	0.02	
Venous resistance (R_v), (mmHg s)/ml	0.0375	0.025	0.015	
Arterial capacitance (C_a), ml/mmHg	0.528	0.792	13	
Venous capacitance (C_v), ml/mmHg	28	42	8	

LV Left ventricle, *RV* right ventricle, *LA* left atrium, *RA* right atrium, *EDPVR* end-diastolic pressure–volume relationship

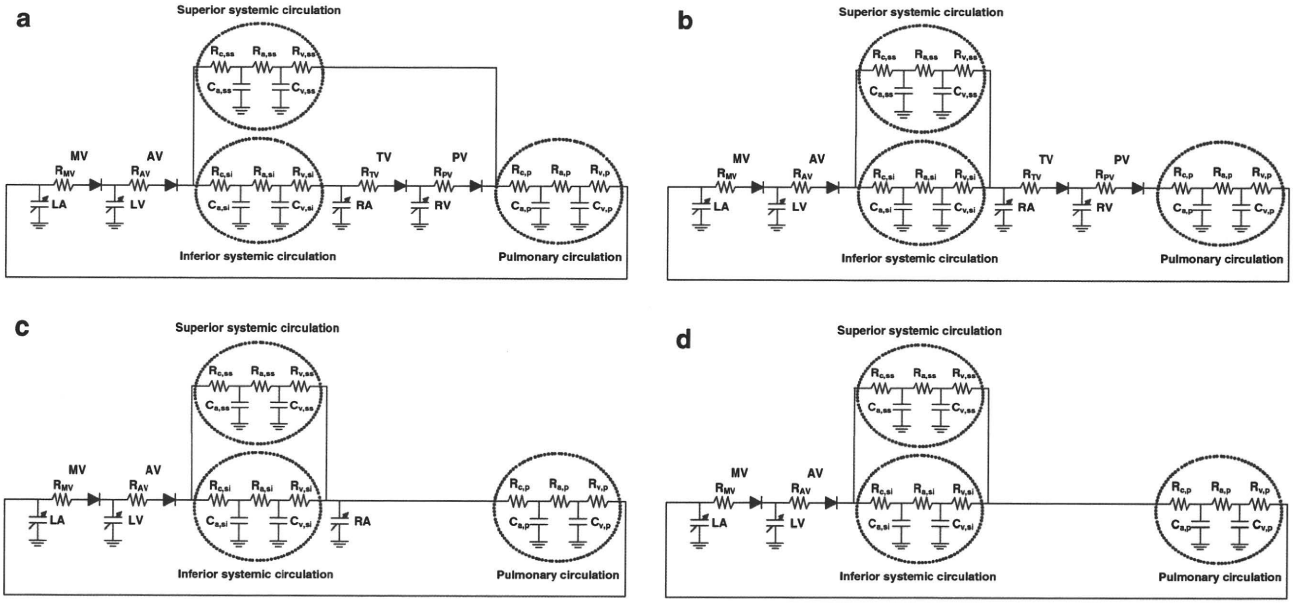

Fig. 1 **a** The electric equivalent circuit of one and a half ventricle repair. **b** Biventricular repair (normal circulation). **c**,**d** Variations of Fontan operation [**c** atriopulmonary connection (APC); **d** total cavopulmonary connection (TCPC)]. *LV* and *RV* left and right ventricles, *LA* and *RA* left and right atria, *AV* and *MV* aortic and mitral valves, *PV* and *TV* pulmonary and tricuspid valves, C_a and C_v lumped arterial and venous capacitances, R_c characteristic impedances, R_a lumped arterial resistances, R_v venous resistances, *ss* superior systemic circulation, *si* inferior systemic circulation, *p* pulmonary circulation

$$e_{cc}(t) = 0.5[1 - \cos(\pi t/T_{es,cc})]\ (0 \le t < 2T_{es,cc})$$
$$e_{cc}(t) = 0\ (2T_{es,cc} \le t < T_c) \quad (3)$$

where t is the time from the start of systole, $T_{es,cc}$ is the duration of systole, and T_c is the duration of cardiac cycle. Using $e_{cc}(t)$, the instantaneous pressure, $P_{cc}(t)$, is described by:

$$P_{cc}(t) = [P_{es,cc}(V_{cc}) - P_{ed,cc}(V_{cc})]e_{cc}(t) + P_{ed,cc}(V_{cc}) \quad (4)$$

Ventricular systole is preceded by atrial systole. The time advance of atrial systole (DT) is calculated as the fixed fraction of T_c (DT = $0.02T_c$). Function of each chamber is characterized by the parameters $E_{es,cc}$, $T_{es,cc}$, $V_{0,cc}$, A_{cc}, B_{cc}, and $e_{cc}(t)$. The same $e_{cc}(t)$ was used for all chambers, but the other parameters were different between chambers, as shown in Table 1.

Vascular system

Basically, the pulmonary and systemic circulations are modeled as modified Windkessel impedances. Each vascular system is modeled by lumped venous (C_v) and arterial (C_a) capacitances, a characteristic impedance (R_c) that is related to the stiffness of the proximal aorta or pulmonary artery, a lumped arterial resistance (R_a), and a resistance proximal to C_v (R_v). This framework is similar to that used in deriving Guyton's resistance to venous return [14].

To simulate the postoperative hemodynamics of 1.5VR, the systemic circulation is divided into two parts, the superior and the inferior circulation. Therefore, the parameters of the systemic circulation are also divided into the superior and inferior ones, as shown in Fig. 1. Blood flow in the descending aorta is reported to be 63.8% of the left ventricular output [15]. The compliance of the IVC is considered to be 66.6% of the total venous compliance [16]. Thus, in our model, arterial and venous compliances of the inferior systemic circulation are adjusted to 0.6 times those of the compliance of the total circulation, and the blood flow of the inferior systemic circulation is controlled to be 60% of the left ventricular output by adjusting the resistances of R_c, R_a, and R_v.

The capacitance of the superior systemic circulation is also divided into arterial ($C_{a,ss}$) and venous ($C_{v,ss}$). Similarly, arterial and venous capacitances are defined for the inferior systemic circulation ($C_{a,si}$ and $C_{v,si}$) and for the pulmonary circulation ($C_{a,p}$ and $C_{v,p}$). The ratio of C_a to C_v was obtained from the literature [9, 10, 13]. The relationship between pressure (P_c) and volume (V_c) in each capacitance is described by the following linear formula.

$$P_c = \frac{V_c}{C} \quad (5)$$

The changes in volume in each capacitance ($dV(t)/dt$) are described by the differential equations below

$$\frac{dV(t)}{dt} = \sum Q_{\text{in-flow}}(t) - \sum Q_{\text{out-flow}}(t) \quad (6)$$

where $\Sigma Q_{\text{in-flow}}(t)$ and $\Sigma Q_{\text{out-flow}}(t)$ indicate the sum of instantaneous volumetric flow rates at the inlet and outlet of each compartment, respectively. Each of the aortic, mitral, pulmonary, and tricuspid valves is described as an ideal diode with a serially connected small resistor.

In the 1.5VR model, the superior circulation flows from SVC to PA, while the inferior blood flow returns to RA through IVC as shown in Fig. 1a. The models of 2VR (Fig. 1b) and variations of Fontan operation [Fig. 1c, atriopulmonary connection (APC); Fig. 1d, total cavopulmonary connection (TCPC)] are constructed for comparisons. Although the superior and inferior systemic circulations return to RA in both 2VR and APC models, RA is directly connected to PA in the APC model. In the TCPC model, SVC and IVC are directly connected to PA. All parameter values were the same for all of these models except total stressed blood volume (see below) (Table 1).

Hypoplastic RV

Hypoplastic RV is physiologically characterized by an increase in RV stiffness caused by hypertrophy and fibroelastosis of RV muscles [6]. Recalling Eq. 2 for RV, we have:

$$P_{\text{ed,RV}} = A_{\text{RV}}\left[e^{B_{\text{RV}}\left(V_{\text{ed,RV}} - V_{0,\text{RV}}\right)} - 1\right] \quad (7)$$

where B_{RV} is stiffness constant of RV. The value of B_{RV} was changed stepwise from 0.023/ml (normal RV) to 0.143/ml (extremely stiff RV) in increments of 0.01/ml to simulate the various degrees of RV stiffness associated with hypoplasia (Fig. 2).

Protocols

First, the control state was simulated by the 2VR model with normal RV stiffness constant ($B_{\text{RV}} = 0.023$). The total stressed blood volume (V_s), equal to the sum of the stressed volumes in each capacitance and the volume of each chamber, was set as 750 ml to reproduce normal hemodynamics.

$$V_s = V_{\text{LV}} + V_{\text{RV}} + V_{\text{LA}} + V_{\text{RA}} + V_{\text{Ca,ss}} + V_{\text{Cv,ss}} + V_{\text{Ca,si}} + V_{\text{Cv,si}} + V_{\text{Ca,p}} + V_{\text{Cv,p}} \quad (8)$$

We solved these simultaneous equations (Eqs. 1–8) using the component ODE45 of MATLAB, based on the Runge–Kutta method (MathWorks). The hemodynamic parameters of 2VR with normal RV stiffness constant are listed in Table 2.

Next, systemic cardiac output, pulmonary arterial pressure (PAP), right atrial pressure (RAP), and RVEDV after each procedure were calculated for each RV stiffness constant. Heart rate was kept constant and mean systemic arterial pressure (MAP) was controlled at the same value as that of the control state, by adjusting the total stressed blood volume.

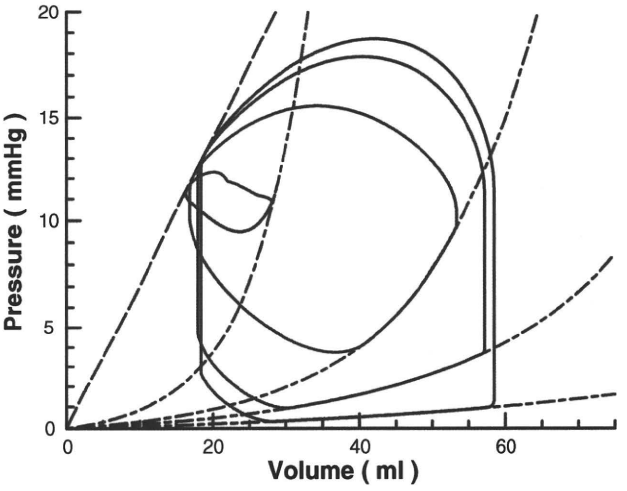

Fig. 2 Right ventricular pressure–volume loops (PV loop) after one and a half ventricle repair. With the increase in the right ventricular stiffness constant, the PV loop became smaller. The *horizontal axis* is the instantaneous right ventricular volume (ml) and the *longitudinal axis* is the instantaneous right ventricular pressure (mmHg)

Table 2 Control hemodynamic parameters (2VR with normal RV stiffness constant)

Parameter	Value
Heart rate (HR), beats/min	75
Mean systemic arterial pressure (MAP), mmHg	80.3
Mean pulmonary arterial pressure (PAP), mmHg	13.6
Mean right atrial pressure (RAP), mmHg	2.34
Mean left atrial pressure (LAP), mmHg	8.26
Left ventricular cardiac output (CO), l/min	4.95

Results

Figure 3a shows the impact of the RV stiffness constant on systemic cardiac output after each procedure. In the Fontan circulation (APC and TCPC), systemic cardiac output was independent of the RV stiffness constant and remained at 4.40 l/min. Under the condition of normal RV stiffness constant, systemic cardiac output was 4.95 l/min in 2VR and 4.73 l/min in 1.5VR, being 13 and 8% greater than that of Fontan circulation, respectively. As the RV stiffness constant was increased from the control value to mimic increased severity of RV

hypoplasia, systemic cardiac output decreased in both 2VR and 1.5VR circulations. Within the range between 100 and 150% of the control RV stiffness constant, systemic cardiac output of 2VR circulation was obviously greater than those of other two circulations. With the RV stiffness constant >150%, systemic cardiac output became greater in 1.5VR than in 2VR. In this situation, 2VR needed larger stressed blood volume than 1.5VR to maintain MAP (Fig. 3d).

The results for PAP and RAP are shown in Fig. 3b. As the RV stiffness constant increased, PAP decreased and RAP increased in both 2VR and 1.5VR circulations. In 2VR circulation, RAP increased steeply as the RV stiffness constant increased up to 150% of normal, and exceeded the atrial pressure of TCPC when the RV stiffness constant increased above 150% of normal. In 1.5VR circulation, RAP also increased but more slowly and exceeded the atrial pressure of TCPC only when the RV stiffness constant increased above 250% of normal. PAP in 1.5VR circulation, which was equal to SVC pressure, became higher than PAP in 2VR circulation in the range of RV stiffness constant >150% of normal.

In the control state, RVEDV in 2VR was 87.7 ml, which was treated as the value of 100% of RVEDV. The influence of the RV stiffness constant on RVEDV is shown in Fig. 3c. In 2VR circulation, RVEDV decreased as the RV stiffness constant increased. In 1.5VR circulation, RVEDV reduced only slightly with an increase in the RV stiffness constant until 250% of normal. In the range of RV stiffness constant >250% of normal, RVEDV showed a relatively linear decay in both 2VR and 1.5VR circulations, and there was no difference in RVEDV between 2VR and 1.5VR. In this situation, both 1.5VR and 2VR needed larger stressed blood volume than Fontan circulation (Fig. 3d).

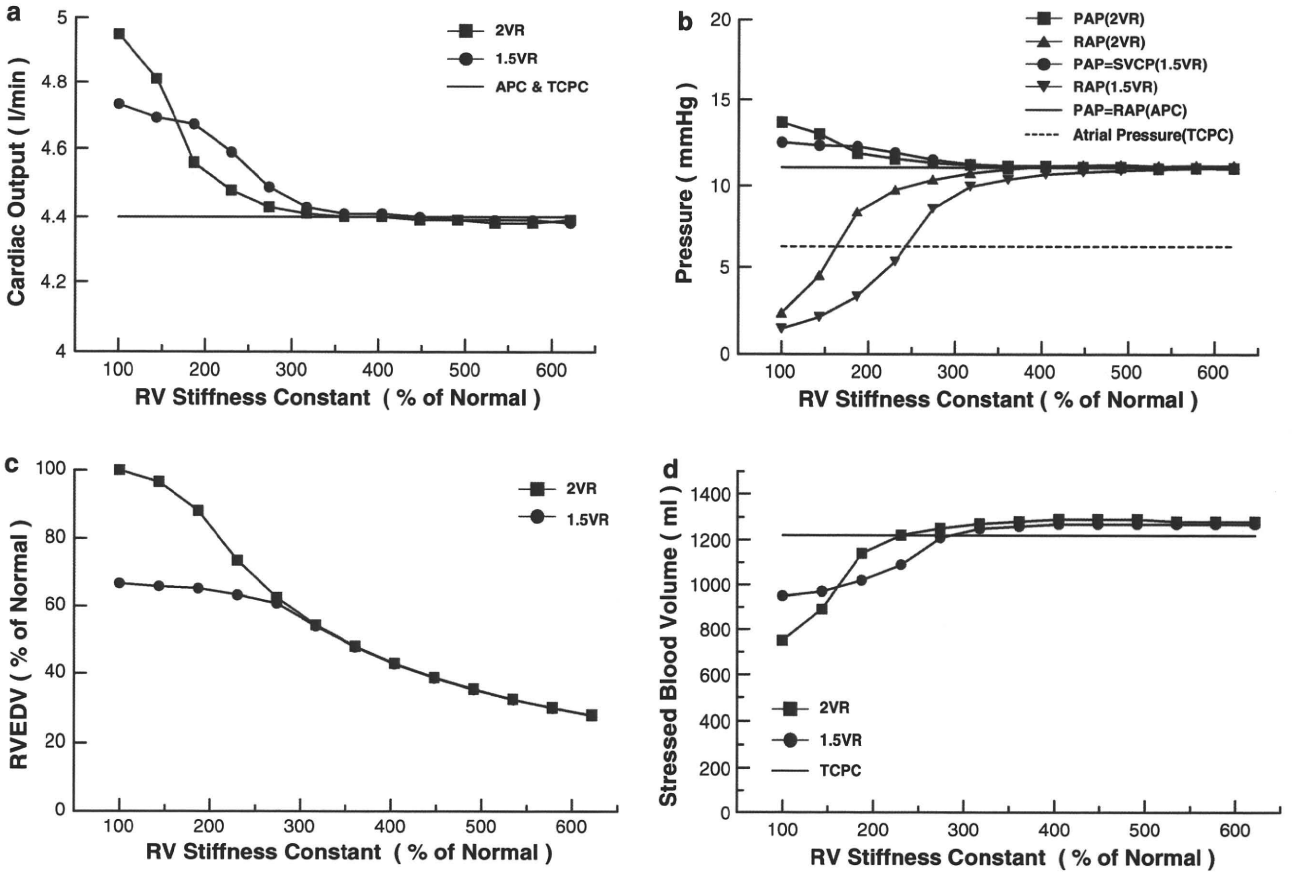

Fig. 3 **a** The relationship between systemic cardiac output (l/min) and % stiffness constant of hypoplastic right ventricle. The *horizontal axis* is the ratio of RV stiffness constant (% stiffness constant) to the normal value. **b** The relationship between pulmonary arterial pressure or right atrial pressure (mmHg) and % stiffness constant of hypoplastic RV. Pulmonary arterial pressure is the same as right atrial pressure in APC. **c** The relationship between % RVEDV and % stiffness constant of hypoplastic RV. **d** The relationship between stressed blood volume (ml) and % stiffness constant. *2VR* biventricular repair, *1.5VR* one and a half ventricle repair, *APC* and *TCPC* variations of Fontan operation (*APC* atriopulmonary connection, *TCPC* total cavopulmonary connection); *PAP* pulmonary arterial pressure, *RAP* right atrial pressure, *SVCP* superior vena caval pressure, *RVEDV* right ventricular end-diastolic volume